March
2005

fea INFORMATION

WWW.FEAINFORMATION.COM

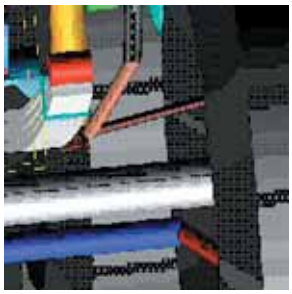

COVER STORY

ANSYS INC.

STRIVE FOR GREENER ENVIRONMENTS

TECHNICAL SPOTLIGHT

ARUP DETROIT

AUTO DESIGN AND

PEDESTRIAN SAFETY

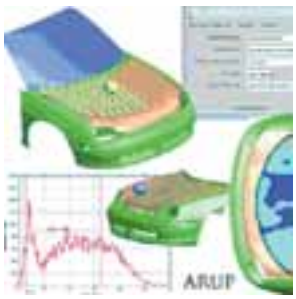

PRODUCT SPOTLIGHT

NEC LAUNCHES WORLD'S FASTEST

VECTOR SUPERCOMPUTER

FEA Information Worldwide Participant's

Contents

FEATURED PUBLICATION: Published by Dr. David Benson

Editor: Trent Eggleston **Managing Editor:** Marsha Victory **Technical Editor:** Art Shapiro **Graphic Designer:** Wayne L. Mindle	**Technical Writers:** Dr. David Benson Uli Franz Ala Tabiei **Technical Consultants:** Steve Pilz Reza Sadeghi

FEA Information Announcements

New Participant to FEA Information Inc. www.feainformation.com

Infinite Simulation Systems B.V.e
Tel: +31 76 578 09 90
Fax: +31 76 578 09 99
Contact: Jurgen Mathijssen - j.mathijssen@infinite.nl
Web: http://www.infinite.nl
Sales, Training, Consulting: ANSYS, LMS Virtual Lab, LS-DYNA

Addition to LS-DYNA Resource Page:

Section dedicated to only LS-DYNA Event dates and locations

Cover Design:

Cameron Design
www.cameron-design.com

Sincerely,
Trent Eggleston & Marsha Victory

Cover Story – ANSYS Inc.

Strive for Greener Environment: HVAC Manufacturer Uses CFX To Improve Energy Efficiency, Reduce Environmental Impact

Trane centrifugal chillers in the chilled water plant at the University of Arizona, Tucson.

EXECUTIVE SUMMARY

Challenge:

To improve energy efficiency in the design of refrigerant-cooled hermetic motors for water- and air-cooled chillers.

Solution:

Implement CFX to simulate heat transfer phenomena in high-power induction motors and refrigerant
flow through the hermetic motors.

Benefits:

Enabled engineers to explore large-scale unsteady flow phenomena to obtain the highest energy efficiency in a wide range of applications.

Minimized environmental impact by improving reliability of the products, increasing service intervals, and reducing the need for disassembly of the units. Also eliminated possible emission of refrigerant associated with these processes.

Using CFX to analyze the unsteady flow field inside the chiller, track down the response of the unit structure, and predict air motion around the machines, allowed engineers to deliver units with lowest noise radiation.

Introduction

As living standards rise precision manufacturing proliferates around the world, air-conditioning equipment accounts for more and more energy consumption. Stricter environmental regulations and increasing environmental consciousness of air conditioning equipment users demand more efficient compressors with less impact on the environment.

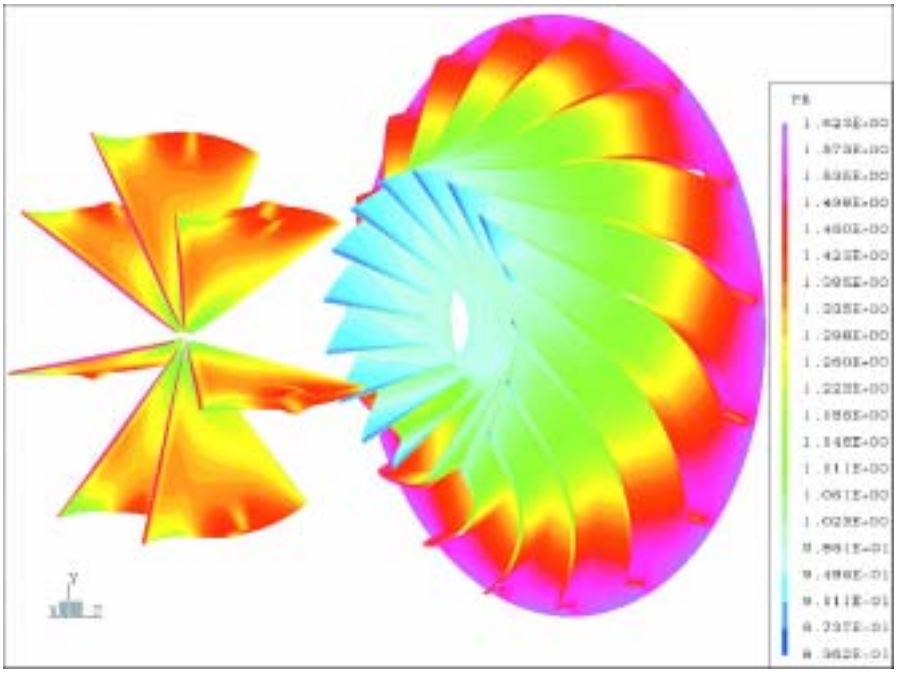

The Trane Company, a leading worldwide supplier of indoor comfort systems, is using the latest technology — CFX software from ANSYS, Inc. — to achieve these goals.

Improving energy efficiency is a key issue in the design of chillers for an air-conditioning system. Efficient chillers not only reduce the operating cost but also reduce green house gas emissions by reducing power consumption. A one-percent increase in efficiency brings substantial savings over the life of a medium size chiller.

The social and environmental benefits are even greater. Trane engineers are using multi-objective optimization to improve chiller efficiency. Different from the traditional trial-and-error technique, Trane engineers analyze multiple variables and effects simultaneously and optimize the design to achieve the maximum benefit.

Challenge:

A refrigerant-cooled hermetic motor is an integral part of Trane water and air-cooled chillers. This technology provides high efficiency and extends the life of high-power induction motors. In these hermetic refrigeration machines, coolant flow is needed to carry away the heat generated by high power motors to improve energy efficiency and motor durability. However, the coolant flow also induces the windage loss to the systems.
Two competing mechanisms need to be quantified simultaneously to achieve the optimized design of these hermetic systems. Trane engineers use latest computational fluid dynamics (CFD) technology to simulate heat transfer phenomena in high-power induction motors and refrigerant flow through these motors concurrently.

These simulations bring many benefits compared to traditional build-and-test techniques: temperature distribution in the motor is evaluated to eliminate hot spots and obtain uniform cooling; through-flow induced torque and loss are determined; the impact of rotor surface geometry and speed are assessed; and the required mass flow rate for effective cooling is predicted. As a result, hermetic refrigerant machines are designed with optimized configuration for the best energy efficiency.

CFX calculates force and torque from pressure and viscous shear stress on the surface of inlet

guide vanes and impeller of a Trane centrifugal compressor stage.

To improve energy efficiency, design and analysis move from the individual component to the entire system. Compressor aerodynamic performance is no longer limited to single parts, but extended to include the interaction of multiple components.

This integrated analysis ensures the maximum performance of each component as a part of the compressor system at various working conditions.

Solution

Trane has developed a Virtual Laboratory for the design of refrigerant compressors. It is based on CFX, a CFD software package that Trane has found to be ideally suited to modeling indoor comfort systems and which includes a real-gas equation of state for the refrigerant. The result is that engineers can easily obtain overall performance and local flow field details for complete compressor stages without building a prototype.

Different from single-component analysis, the Trane Virtual Laboratory simulates the entire compressor, readily providing information on the interactions between the components. Since it quantifies the impact of design changes of a single part on the performance of the whole compressor, this feature has special value for the overall improvement of machines. This capacity proved very useful when Trane investigated the options to use different diffusers in compressors.

The impact on the overall compressor performance was analyzed in detail, with the simulations indicating that the change would lead to different flow fields inside the upstream and downstream components. The individual performance of these components was altered when the diffuser was changed. The information obtained was of great value to designers, guiding product improvements and avoiding unnecessary design iterations.

Transient simulations in the Trane Virtual Laboratory provide further physical insights into compressor performance and flow field unsteadiness, reduction of which is critical to improve efficiency and reduce vibration and noise levels. Pressure fluctuation distributions inside the impellers and diffusers can be obtained for different compressor designs and loss mechanisms inside the flow field can be studied thoroughly.

CFX allows Trane engineers to explore large-scale unsteady flow phenomena. Removing these instabilities has the benefit of obtaining the highest energy efficiency in a wide range of applications. To minimize the impact on the environment, Trane also develops technology to improve the reliability of our products, increase service intervals, and reduce the need for disassembly of the units. Possible emission of refrigerant associated with these processes is eliminated.

For the compressors designed by Trane, the force and torque on components are quantified to ensure safety and reliability. The force and torque are calculated from the pressure and viscous shear stress obtained from flow field simulations on the surface of the components. These force and torque calculations are also used to predict the vibration and noise of the system. The possibility of failure associated with fatigue of the components is therefore reduced. All this analysis is conducted using a whole system simulation under strict dynamic loading conditions. This cutting-edge technology helps Trane chillers earn a reputation as the world's most reliable refrigeration machines.

In recent years, the sound produced by HVAC equipment has attracted more attention. Since the equipment is typically located near building occupants, noise radiation must be controlled. Reducing acoustic impact is particularly important for hospitals, schools, and music halls.

The machinery sound from HVAC equipment is caused by temporal variation in the flow field.

The internal flow field vibrates the machines, setting the air around them in motion. This unsteadiness reaches the human ear in the form of noise.

Benefits

By using CFX to analyze the unsteady flow field inside the chiller, track down the response of the unit structure, and predict air motion around the machines, Trane engineers deliver units with the lowest noise radiation. Since Trane developed the industrial first scroll compressor, the Trane 3-D® scroll compressor, in 1987, these devices have dominated the market for small tonnage air-conditioning equipment.

Compared to the reciprocating compressors, where intake, compression, and discharge occur in discrete steps, scroll compressors conduct intake, compression, and discharge phases of operation simultaneously in an ongoing sequence. Their smooth operating characteristics reduce force and torque variation inside the compressor, making scroll compressors quiet and reliable. Lubrication is very critical to improve the durability of scroll compressors since the oil pump is an integral part of the compressor. Trane engineers developed the technology to use the latest particle tracking techniques to predict the oil circulation rate inside the scroll compressors.

The oil coming from different regions inside the compressors is tracked through the operating process. Oil circulation features of different designs and oil droplet sizes are obtained at different operating conditions.

CFX helps designers develop compressor designs with adequate lubrication and an ample supply of oil. The fully lubricated moving components extend the durability of the system and reduce the need to replace parts and service the units.

Technical Spotlight:

An automotive design engineering provider uses LS-DYNA to make CAE more efficient and keep pedestrians safer.

By Simon Hart, Arup Detroit Vehicle Design Group office

Reproduced with permission of Desktop Engineering Magazine, a Helmers Publishing Inc. publication, www.deskeng.com

Beginning in late 2005, car makers won't be able to sell autos in Europe unless they pass new tests to show their front ends are safer for pedestrians. In European Union (EU) countries nearly a fifth of all traffic deaths are pedestrians—9,000 per year—and 80 percent of them occur when the victim's head hits the hood or windshield at an average vehicle speed of 25 mph.And while improvements in design have led to fewer driver and passenger injuries, pedestrian injuries and fatalities now account for about 30 percent of the overall number in Europe. As a result, the new EU tests (Directive 2003/102/EC) will cover head and leg impacts involving the bumper, hood, windshield, and A-pillar. Japan will require the tests in 2007, and the requirements will become more challenging in 2010, when a further phase of requirements takes effect in Europe.

Though the US National Highway Safety Administration has said pedestrian deaths account for 11 percent of all motor vehicle fatalities in the US, the European market remains important for US manufacturers.

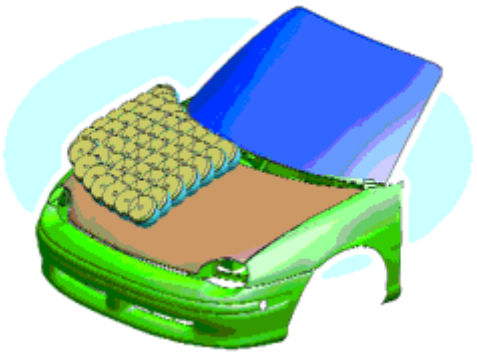

An Analysis Pickle

The regulations have major implications for the design of vehicles now that the hood and bumper must be designed to absorb the energy of impacts at relatively low loads. The pedestrian impact tests consist of propelling test devices representing adult and child heads and leg parts into the fronts of stationary vehicles. Instrumentation reports the accelerations and loads during the impact.

While modelling the tests for finite element analysis (FEA) takes a similar approach to the analysis of a crash event, it stands in contrast to the crashworthiness requirements that have shaped vehicle structures in recent decades. To perform well in crash tests, front structures must be stiff and deform at high loads to protect the occupants inside. Additionally, the free space between ex-

terior panels and the interior components of a modern vehicle has been reduced through efficient packaging and styling trends.

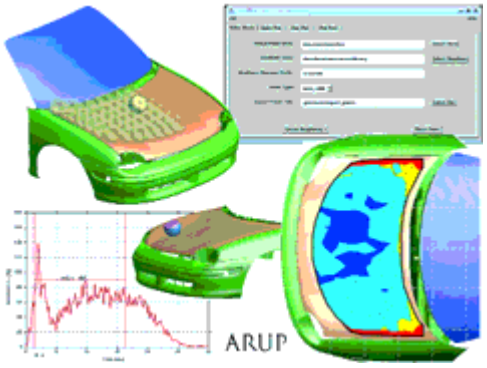

Arup Vehicle Design Group uses automated processes for model creation and post processing of results for pedestrian impact analysis. The multicolored hood shows impact zones with contoured plot results.

Because of this, if the structure could deform at a low enough load, it would not be able to deflect far enough to absorb the energy of a pedestrian impact. Further complications arise from the need to have exterior panels that are dent resistant, a hood closure of adequate stiffness, and a bumper system that can withstand low speed impacts.

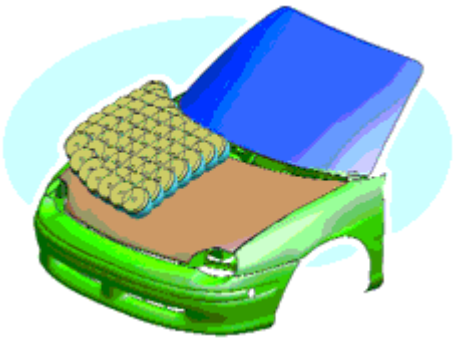

The headform model is positioned automatically for analysis of multiple impact locations

As a result, the solution seems to be to allow for extra space between surfaces on top of what is necessary to fulfill traditional requirements. Bumpers will be deeper and softer and hoods will be higher with more space between them and the car's engine and suspension towers.

The engineers responsible for analyzing vehicle structures are now faced with increasing numbers of analyses to perform. Because of simulations, extracting results, limited computing resources, and repeated simulations due to modelling errors, engineers run the risk of being sucked into a cycle of constant model updating and reanalysis. That means CAE becomes a burden.

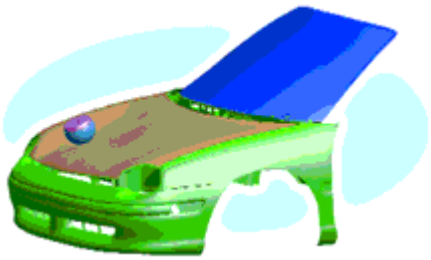

Front end model set up for a head impact analysis.

Saving Time in the Process

But some innovators in CAE have recognized this problem and Arup Vehicle Design Group located in Birmingham, England, has developed an approach that automates large portions of this analysis process. This means engineers will be able to design new vehicle front ends to meet the new regulations.Arup, using LS-DYNA—developed by Livermore Soft-

ware Technology Corporation (LSTC) in Livermore, Calif.—as its finite element solver and Arup's own Oasys Primer, D3PLOT, and T/HIS software packages for postprocessing results, streamlined the usual approach to make it more efficient. While many tasks in simulation are repetitive and time consuming, they nevertheless require careful control to avoid errors. Programmers recognized that automating these tasks—a few include preparing different load cases, error checking, and extracting results—would save time.

In the case of pedestrian protection, Arup Vehicle Design Group developed a process that lets engineers quickly assess the performance of their designs. A computer program manages the analysis process and reduces the user input necessary for multiple model creation and execution. It can automatically prepare and submit models for analysis and present key results to the user.

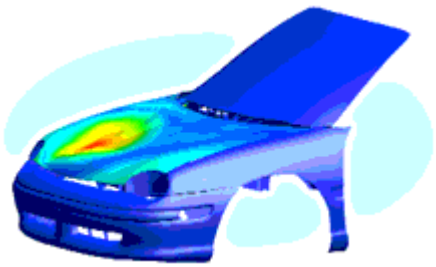

Contour plot showing displacement results for a head impact analysis.

Applying Advanced CAE to Pedestrian Impacts

Under the 2005 directive, two-thirds of the car's hood must help limit pedestrian head injuries by reducing acceleration. This can be accomplished by designing exterior car surfaces with more flexible materials and ensuring there is sufficient space below the surface to allow it to deform without contacting rigid components. To be sure of compliance, engineers must test every possible point of impact, leading to hundreds of analyses for every hood design. Several design iterations are typical in auto design, so it is easy to see the benefit of a package that automates part of the process.

The vehicle model is specified on a graphical interface and the test device is chosen from a library. The user can submit a file of x, y coordinates and the location of the impact point in 3D space will be calculated automatically. Input data is generated for every impact point and written to a subdirectory structure. Execution of the models is automatic. After analyses are completed, automatic postprocessing extracts critical data—in this case head injury criteria (HIC). This data is presented as a colored plot of the impact zone, so that problem areas can be identified. The percentage area of the impact zone that meets the directive targets can also be calculated from this data.

Arup develops its own library of pedestrian test device models, which correlate with the actual devices and test data from vehicle tests when they are available. The Arup program can also be used to manage analysis of the upper and lower legform pedestrian tests.

Arup has used this process on vehicle programs with great success. It has allowed rapid response during the most critical stages of design, by bypassing

the traditional bottlenecks in the analysis process. Arup is continually developing its range of analysis tools with the goal of pushing CAE forward to meet the challenges of modern vehicle design.

Simon Hart *joined Arup in 1994 and works in the Detroit Vehicle Design Group office, providing analysis and engineering services to automotive OEMs and suppliers..*

Product information

LS-Dyna
Livermore Software Technology
Corp.
Livermore, CA
lstc.com

Arup Vehicle Design Group
Detroit, MI and Birmingham, UK

Product Spotlight – NEC www.nec.com

NEC Launches World's Fastest Vector Supercomputer

SX Series Model "SX-8"

Supercomputer SX-8 Series (Multi-Node System)"

NEC Corporation's "SX-8," the world's most powerful vector supercomputer with a peak processing performance of 65TFLOPS (TFLOPS: one trillion floating point operations per second).

Inheriting vector architecture, whose excellent sustained performance has been demonstrated by the Earth Simulator, the new product combines enhanced CPUs, and memory and I/O processing performance. A further-enhanced, single-chip, vector processor, realized by the SX-6, also contributes to the greatly improved price performance and space saving offered by the SX-8.

The SX-8, with its dedicated CPUs, large-scale memory, and high data transfer rate between memory and CPUs, delivers much higher sustained performance than scalar supercomputers with a number of general-purpose CPUs. This is particularly effective in fields that require large-scale and ultra high-speed computing of massive data, such as meteorological forecasting, environmental simulations and automotive crash analysis.

Features of the new product are described below.

1. **World's highest computing performance of 65TFLOPS.**

   The single-node model (includes up to 8 CPUs) achieves a peak vector performance of 128GFLOPS (GFLOPS: one billion floating point operations per second), while the multi-node model achieves the world's fastest peak vector performance of 65TFLOPS when configured with 512 nodes. In addition, a 262TB/s (36.8TB/s in SX-6) high peak data transfer rate between CPU(s) and memory is realized, and it also boasts an enlarged memory capacity of up to 64TB (16TB in SX-6).

2. **Further-enhanced single-chip, vector processor**

The vector processor (vector and scalar units) is integrated into a single chip by applying leading-edge CMOS technology with 90-nanometer (nanometer: 10-9 meter) copper interconnects and the most advanced LSI design technology. Pipelines of the vector unit, the central part of a vector processor, operate at a 2GHz clock frequency, which is double the speed of the SX-6, and realize a peak vector performance of 16GFLOPS per CPU.

Moreover, hardware support of the vector square root operation achieves a sustained performance six times higher than that of the SX-6.

3. Excellent space-saving and power-saving

The SX-8 achieves a reduction in space by 25% and power consumption by 50% as compared with conventional models. This was achieved by applying high-density packaging technology in which processor(s) and memory are implemented on a single module.

4. Software environment suitable for large-scale, multi-node system.

The basic software, "SUPER-UX," maintains upward compatibility with the existing SX series, and achieves further scalability expansion due to enhanced I/O processing and MPI. Global File System (GFS), a high-speed, file sharing system among multiple nodes on a system or among different systems, has also been enhanced. By utilizing GFS, users can access the shared files with a high performance close to that of a local disc, and can also take advantage of the high performance functions of GFS from third party platforms such as SUN and HP as they do with NFS (Network File System).

The monthly rental price of the SX-8 starts from approximately 1,170,000 yen, and shipment commenced in December 2004.

NEC aims to achieve worldwide sales of more than 700 SX-8 units for the next three years. In 1983, NEC entered the market of supercomputers with the launch of SX-2, whose performance exceeded 1GFLOPS for the first time ever, to meet the needs of ultra high-speed scientific computation. Since then, NEC has received over 700 orders across the SX series for their high sustained performance and excellent price performance.

Supercomputers have been utilized for various fields including the development of advanced technology such as functional device materials with nanotechnology, large-scale scientific computing and simulation for energy development such as nuclear fusion, aeronautics and space development, and engineering such as automotive design and development of electronic products.

Recently, while the scale of the problems to be solved becomes larger, a reduction in the development period is ever in-

creasingly desired. Requirements for increase in speed of problem analysis, design, and optimization, have also become more demanding, leading to the need for faster supercomputers.

To respond to these needs, NEC has developed the new vector supercomputer, which boasts greatly improved operating and price performance in comparison with scalar servers that are used for large-scale and large-capacity scientific computing.

Please refer to the appendix for the specifications of the SX-8.

<Appendix> SX-8 Specifications

Specifications			
	Multi-node	Single-node	
	2 - 512 nodes	1 node	
	SX-8/M	SX-8/A	SX-8/B
Central Processing Unit (CPU)			
Number of CPUs	8 - 4,096	4 - 8	1-4
Logical Peak Performance	176G - 90TFLOPS	88G - 176GFLOPS	22G - 88GFLOPS
	(22GFLOPS/CPU)	(22GFLOPS/CPU)	(22GFLOPS/CPU)
Peak Vector Performance	128G - 65TFLOPS	64G - 128GFLOPS	16G - 64GFLOPS
	(16GFLOPS/CPU)	(16GFLOPS/CPU)	(16GFLOPS/CPU)
Main Memory Unit (MMU)			
Memory Architecture	Shared and distributed memory	Shared memory	
Capacity	64G - 64TB	32G - 128GB	16G - 64GB
Peak Data Transfer Rate	262TB/s	512GB/s	256GB/s
Internode Crossbar Switch (IXS)			
Peak Data Transfer Rate	16GB/s x bidirectional (per node	-	

REFERENCE

Vector supercomputer:
A supercomputer with high-speed processor(s) called "vector processor(s)" that is used for scientific/technical computation. Vector supercomputers deliver high performance in complex, large-scale computation, such as fluid dynamics, through the processing of array-handling with a single vector instruction.

A supercomputer with multiple general purpose processors suitable for simultaneous processing of multiple workloads such as genomic analysis or easily paralleled computations like particle computation. They deliver high performance by connecting many processors (also used for business applications) in parallel.

Scalar parallel supercomputer:

AVI Spotlight:

The project is devoted to Finite Element (FE) analysis of topical problems

Full article is located on **www.ls-dyna.com**: menu link: Structures

AVI # 611

Direct Finite Element Modeling of the Radiotelescope RT-70 Mechanics

Borovkov A.I., Shevchenko D.V.

The Complete AVI Libarary is located at **www.feainformation.com** menu link Avi Lib

Industry News – March 2005

M. Victory

Boeing News Release © Boeing www.boeing.com

Boeing 777-200LR, World's Longest-Range Airplane, Makes First Flight

EVERETT, Wash., March 8, 2005 -- The first Boeing [NYSE:BA] 777-200LR World-liner, the world's longest range commercial airplane, today completed its first flight and began a test program that will lead to its first delivery in January 2006.

The newest 777 took off from Everett, Wash., Paine Field at 10 a.m. local time. After approximately three hours, it landed at 1:02 p.m. at Seattle's Boeing Field.

Capts. Suzanna Darcy-Hennemann and Frank Santoni flew the airplane, which carries the distinctive new blue Boeing livery.

Darcy-Hennemann is the 777-200LR project pilot and Santoni is the chief 777 program pilot for Boeing Commercial Airplanes.

"The 777-200LR's ability to connect the world is amazing," Darcy-Hennemann said. "Flying the first flight is an honor and a rare opportunity."

The 777-200LR, capable of connecting virtually any two cities in the world nonstop, is the fifth 777 model. It can carry 301 passengers up to 9,420 nautical miles (17,445 kilometers).

During today's flight, Darcy-Hennemann and Santoni took the airplane to an altitude of 15,000 feet (4,572 meters) and an air speed of 270 knots, or about 310 miles (500 kilometers) per hour, customary on a first flight. Typically, the 777's cruise altitude is 35,000 feet (10,668 meters), and its cruise speed is Mach 0.84, about 484 miles (779 kilometers) per hour.

Darcy-Hennemann and Santoni tested some of the airplane's systems and structures, as on-board equipment recorded and transmit-ted real-time data to a flight-test team at Boeing Field.

The flight-test program will involve the airplane flown today and a second one that's being built. Those will prove the airplane's safety, reliability and service-ready condition during 500 flight hours and 300 ground test hours.

"We expect the 777-200LR to perform splendidly during flight test," said Lars Andersen, vice president - program manager, 777 program, Boeing Commercial Airplanes. "This airplane will carry 20 more passengers, offer 12 percent more revenue cargo volume, consume 25 percent less fuel per seat, and fly 600 nautical miles farther than the competition, the A340-500."

Certification by the U.S. Federal Aviation Administration and Europe's Joint Aviation Authority is expected during the fourth quarter. The first 777-200LR Worldliner is to be delivered to Pakistan International Airlines. EVA Airways is also a launch customer.

Both the 777-200LR and 777-300ER (Extended Range) were launched in February 2002 by Boeing and GE Aircraft Engines at the request of airlines that wanted an airplane with additional flexibility to serve the nonstop routes passengers demand. GE Aircraft Engines makes the 777-200LR Worldliner's engines.

The 777 family has captured over 60 percent of the market since the airplane's October 1990 launch. More than 38 customers worldwide have ordered more than 680 777s, including 112 Longer-Range 777s (777-300ERs and 777-200LRs). So far, two customers have ordered five 777-200LRs.

Asia Pacific News
This month – AMD – MSC.Software CHINA

SUZHOU, China

AMD Opens New Test, Mark And Pack Manufacturing Facility In Suzhou, China

SUZHOU, China -- March 2, 2005 --AMD (NYSE: AMD) today officially opened its new microprocessor test, mark and pack (TMP) facility in Suzhou Industrial Park, China. The new facility, which began rolling out products last December, occupies 11,000 square meters and is located adjacent to Spansion (China) Limited's existing Flash memory assembly and TMP building.

AMD has committed to investing a total of US $33.4 million in the TMP facility through 2009 and has received approval from the Chinese government for a total investment of up to US $100 million. AMD also plans to hire approximately 300 new employees to staff the facility during the next few years.

"Suzhou holds a unique position as one of the key IT manufacturing centers in China and is a key focal point for our global operations," said AMD Chairman, President and CEO, Hector Ruiz. "With software and silicon driving the modern economy, information technology is providing the foundation for China's ability to remain one of the world's brightest lights. At AMD, we are committed to helping China grow in this way."

MSC.Software China - http://www.mscsoftware.com.cn/

Dilip Bhalsod of LSTC, US had a successful trip to China, teaching Advanced LS-DYNA Training for Automotive Crash Analysis to MSC.Software engineers and engineers attending from the Automotive Industy. For LS-DYNA training in China taught by LSTC engineers contact: **pho@lstc.com** For pricing and a 30-day demonstration license of LS-DYNA contact msc.contact@mscsoftware.com.cn

Available Publications on Crash/Safety

mv@feainformation.com

8th International LS-DYNA Users Conference

Prediction of Seat Deformation in Rear Crash Using LS-DYNA
Biswanath Nandi,
Lear Corporation

An Evaluation of Active Knee Bolsters
Zane Z. Yang,
Delphi Corporation

Study of a Driver Airbag Out-Of-Position Using ALE Coupling
Wenyu Lian,
General Motors

A Benchmark Study of CAE Sensor Modeling Using LS-DYNA
C.C. Chou,
Passive Safety R&A,
Ford Motor Company

A FE Modeling and Validation of Vehicle Rubber Mount Preloading and Impact Response
SAE U. Park,
DaimlerChrysler Corporation

IIHS Side Impact Analysis Using LS-DYNA/Madymo Coupling
Jiri Kral,
TNO Madymo North America

Strain Rates in Crashworthiness
Moisey B. Shkolnikov

Influence of Pre-stressed Parts in Dummy Modeling – Simple Considerations
Ulrich Franz
DYNA*more*

Implementation of Modal Represenation for Full Vehicle VPG Simulations
Xianggang Zhang
Engineering Technology AssociatesInc.

FEM for Impact Energy Absorption with Safety Plastic
Iulian Lupea
The Oakwood Group

Curved Barrier Impact of a NASCAR Series Stock Car
Eric A. Nelson
Altair Engineering

Development of a Hybrid Absorbing Reusable Terminal (HEART) Using Finite Element Modeling in LS-DYNA for Roadside Safety Applications
Nauman M. Sheikh
Texas Transportation Inst.
The Texas A&M Univ. Syst.

A Numerical Investigation into H1C and Nij of Children for Forward and Rearward Facing Configurations in a Child Restraint System
William Altenhof
Dept. Mechanical, Automotive and Materials Engineering
University of Windsor

EVENTS

April 5-7, 2005
Westec 2005 Technical Conference - Los Angeles, California, USA

April 11-14, 2005
SAE Global Congress - Detroit, Michigan, USA

May 10, 2005
16th Annual HP Technology Trend in Automotive Engineering Symposium - Plymouth, MI

May 31 – June 03, 2005
Dresden, Germany
Third Joint ANSYS CFX & FZR Workshop on Multiphase Flows

May 17-20, 2005
LeMeridien, St. Julians, Malta
NAFEMS World Congress

May 25-26, 2005
5th European LS-DYNA Conference
The ICC, Birmingham UK (ARUP)

June 06-09, 2005
Westin Harbour Castle, Toronto, Ontario, Canada
AIAA Fluid Dynamics Conference & Exhibit

June 6-10, 2005
HP Software Forum, Denver, CO

June 13-17, 2005
Group (SGIUG) – Munich Germany

June 25-27, 2005
8th U.S. National Congress on Computational Mechanics, Austin, TX

October 20-21
German-LS-DYNA Forum (DYNAmore)
Bamberg, Germany

November 09-11, 2005
23rd CADFEM Users' Meeting – Int'l Congress on FEM Tech. W/ANSYS CFX & ICEM CFD Conference, Bonn, Germany

November 25
Korean Users Conferece – LS-DYNA (THEME)

November 29-30, 2005
Japanese Users Conference (Nagoya) LS-DYNA (JRI)

June 2006
LS-DYNA
9th International LS-DYNA Users Conference – Deerborn, MI (LSTC)

LS-DYNA Resource Page

Interface - Hardware - OS And General Information

LS-DYNA General Information- www.lstc.com sales@lstc.com

Version: 970

Classes:
www.lstc.com classes

30-day demonstration licenses available – no fee

Sales
sales@lstc.com

Participant Hardware and OS that run LS-DYNA (alpha order)

All Hardware and OS listed have been fully QA'd by Livermore Software Technology Corporation

AMD Opteron Linux	HP PA8000 HPUX	INTEL IA32 Linux, Windows	SGI Mips IRIX6.5
CRAY XD1 Linux	HPIA64 HPUX or Linux	INTEL IA64 Linux	SGI IA64 Altix
FUJITSU Prime Power SUN OS 5.8	HP Alpha True 64	INTEL Xeon EMT64 Linux	
FUJITSU VPP Unix System V	IBM Power 4/5 AIX 5.1	NEC SX6 Super-UX	

LS-DYNA Resource Page

Participant Software Interfacing or embedding LS-DYNA

Each software program can interface to all, or a very specific and limited segment of the other software program. The following list are software programs interfacing to or having the LS-DYNA solver embedded within their product. For complete information on the software products visit the corporate website.

ANSYS - ANSYS/LS-DYNA

www.ansys.com/products/environment.asp

ANSYS/LS-DYNA - Built upon the successful ANSYS interface, ANSYS/LS-DYNA is an integrated pre and postprocessor for the worlds most respected explicit dynamics solver, LS-DYNA. The combination makes it possible to solve combined explicit/implicit simulations in a very efficient manner, as well as perform extensive coupled simulations in Robust Design by using mature structural, thermal, electromagnetic and CFD technologies.

AI*Environment: A high end pre and post processor for LS-DYNA, AI*Environment is a powerful tool for advanced modeling of complex structures found in automotive, aerospace, electronic and medical fields. Solid, Shell, Beam, Fluid and Electromagnetic meshing and mesh editing tools are included under a single interface, making AI*Environement highly capable, yet easy to use for advanced modeling needs.

ETA – DYNAFORM

www.eta.com

Includes a complete CAD interface capable of importing, modeling and analyzing, any die design. Available for PC, LINUX and UNIX, DYNAFORM couples affordable software with today's high-end, low-cost hardware for a complete and affordable metal forming solution.

ETA – VPG

www.eta.com

Streamlined CAE software package provides an event-based simulation solution of nonlinear, dynamic problems. eta/VPG's single software package overcomes the limitations of existing CAE analysis methods. It is designed to analyze the behavior of mechanical and structural systems as simple as linkages, and as complex as full vehicles

MSC.Software

“MSC.Dytran LS-DYNA”

www.msc.software.com

Tightly-integrated solution that combines MSC.Dytran's advanced fluid-structure interaction capabilities with LS-DYNA's high-performance structural DMP within a common simulation environment. Innovative explicit nonlinear technology enables extreme, short-duration dynamic events to be simulated for a variety of industrial and commercial applications on UNIX, Linux, and Windows platforms. Joint solution can also be used in conjunction with a full suite of Virtual Product Development tools via a flexible, cost-effective MSC.MasterKey License System.

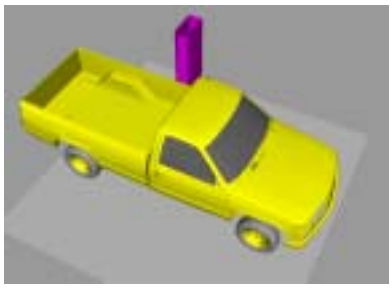

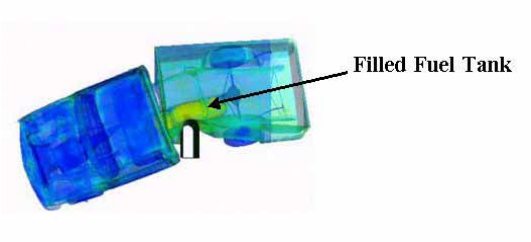

Side Impact With Fuel Oil Inside

MSC.Software - MSC.Nastran/SOL 700

The MSC.Nastran™ Explicit Nonlinear product module (SOL 700) provides MSC.Nastran users the ability access the explicit nonlinear structural simulation capabilities of the MSC.Dytran LS-DYNA solver using the MSC.Nastran Bulk Data input format. This product module offers unprecedented capabilities to analyze a variety of problems involving short duration, highly dynamic events with severe geometric and material nonlinearities.

MSC.Nastran Explicit Nonlinear will allow users to work within one common modeling environment using the same Bulk Data interface. NVH, linear, and nonlinear models can be used for explicit applications such as crash, crush, and drop test simulations. This reduces the time required to build additional models for another analysis programs, lowers risk due to information transfer or translation issues, and eliminates the need for additional software training.
The MSC.Nastran Sol 700 will be released in November 2005. Beta release is available now !

MSC.Software – Gateway for LS-DYNA

Gateway for LS-DYNA provides you with the ability to access basic LS-DYNA simulation capabilities in a fully integrated and generative way. Accessed via a specific Crash workbench on the GPS workspace, the application enhances CATIA V5 to allow finite element analysis models to be output to LS-DYNA and then results to be displayed back in CATIA. Gateway for LS-DYNA supports explicit nonlinear analysis such as crash, drop test, and rigid wall analysis.

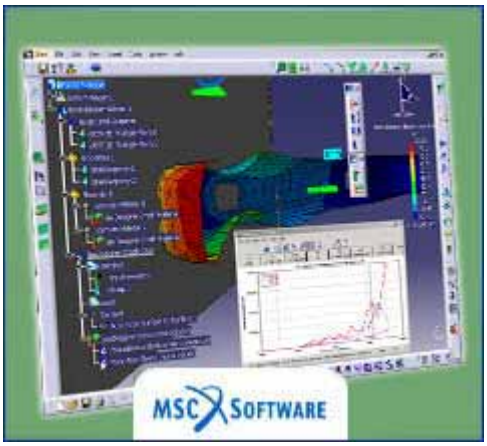

Gateway products provide CATIA V5 users with the ability to directly interface with their existing corporate simulation resources, and exchange and archive associated simulation data.

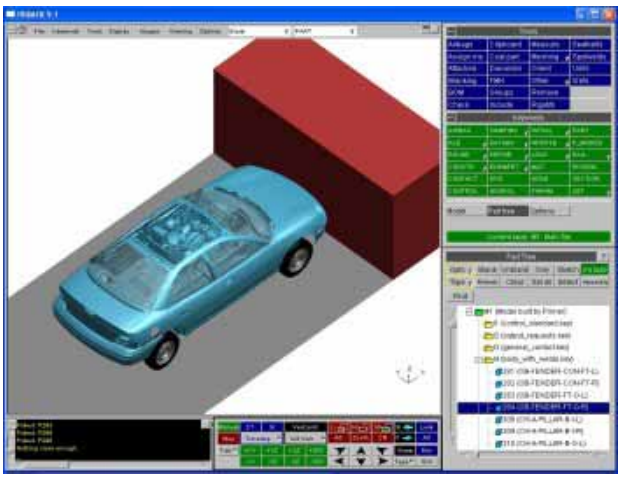

Oasys software for LS-DYNA
www.arup.com/dyna

Oasys software is custom-written for 100% compatibility with LS-DYNA. Oasys PRIMER offers model creation, editing and error removal, together with many specialist functions for rapid generation of error-free models. Oasys also offer post-processing software for in-depth analysis of results and automatic report generation.

LS-DYNA Events

UK 05/25-26/05 (Arup)
5th European LS-DYNA Conference

Germany - 10/20-10/21 (DYNAmore)
German LS-DYNA Forum

Germany - 11/09-11/11 (CADFEM)
Int'l Congress on FEM Tech.. workshops focusing on LS-DYNA

Korea 11/25/05 (THEME)
Korean LS-DYNA Users Conference

Japan 11/29-30/05 (JRI)
Japanese LS-DYNA Users Conference (Nagoya)

US 06/06 (LSTC)
9th International LS-DYNA Users Conference

Hardware & Computing and Communication Products

www.amd.com

www.fujitsu.com

www.hp.com

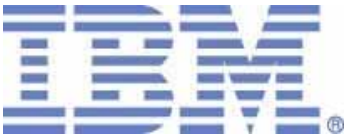

www-1.ibm.com/servers/deepcomputing

www.intel.com

www.nec.com

www.sgi.com

www.cray.com

Software Distributors

Alphabetical order by Country

Australia	**Leading Engineering Analysis Providers** www.leapaust.com.au
Canada	**Metal Forming Analysis Corporation** www.mfac.com
China	**ANSYS China** www.ansys.cn
China	**MSC. Software – China** www.mscsoftware.com.cn
Germany	**CAD-FEM** www.cadfem.de
Germany	**Dyna*More*** www.dynamore.de
India	**GissETA** www.gisseta.com
India	**Altair Engineering India** www.altair.com
Italy	**Altair Engineering Italy** www.altairtorino.it
Italy	**Numerica SRL** www.numerica-srl.it
Japan	**Fujitsu Limited** www.fujitsu.com
Japan	**The Japan Research Institute** www.jri.co.jp
Japan	**CRC Solutions Corp.** www.engineering-eye.com
Korea	**Korean Simulation Technologies** www.kostech.co.kr
Korea	**Theme Engineering** www.lsdyna.co.kr

Software Distributors (cont.)

Alphabetical order by Country

Netherlands	**Infinite Simulation Systems B.V** www.infinite.nl
Russia	**Strela, LLC** www.ls-dynarussia.com
Sweden	**Engineering Research AB** www.erab.se
Taiwan	**Flotrend** www.flotrend.com.tw
Turkey	**FIGES** www.figes.com.tr
USA	**Altair Western Region** www.altair.com
USA	**Engineering Technology Associates** www.eta.com
USA	**Dynamax** www.dynamax-inc.com
USA	**Livermore Software Technology Corp.** www.lstc.com
USA	**ANSYS Inc.** www.ansys.com
UK	**Oasys, LTC** www.arup.com/dyna/

Consulting and Engineering Services

Alphabetical Order By Country

Australia Manly, NSW www.leapaust.com.au	**Leading Engineering Analysis Providers** Greg Horner info@leapaust.com.au 02 8966 7888
Canada Kingston, Ontario www.mfac.com	**Metal Forming Analysis Corporation** Chris Galbraith galb@mfac.com (613) 547-5395
India Bangalore www.altair.com	**Altair Engineering India** Nelson Dias info-in@altair.com 91 (0)80 2658-8540
Italy Torino www.altairtorino.it	**Altair Engineering Italy** sales@altairtorino.it
Italy Firenze www.numerica-srl.it	**Numerica SRL** info@numerica-srl.it 39 055 432010
UK Solihull, West Midlands www.arup.com	**ARUP** Brian Walker brian.walker@arup.com 44 (0) 121 213 3317
USA Irvine, CA www.altair.com	**Altair Engineering Inc. Western Region** Harold Thomas info-ca@altair.com
USA Windsor, CA www.schwer.net/SECS	**SE&CS** Len Schwer len@schwer.net (707) 837-0559

Educational & Contributing Participants

Alphabetical Order By Country

China	Dr. Quing Zhou	Tsinghua University
India	Dr. Anindya Deb	Indian Institute of Science
Italy	Professor Gennaro Monacelli	Prode – Elasis & Univ. of Napoli, Frederico II
Russia	Dr. Alexey I. Borovkov	St. Petersburg State Tech. University
USA	Dr. Ted Belytschko	Northwestern University
USA	Dr. David Benson	University of California – San Diego
USA	Dr. Bhavin V. Mehta	Ohio University
USA	Dr. Taylan Altan	The Ohio State U – ERC/NSM
USA	Dr. Ala Tabiei	University of Cincinnati
USA	Tony Taylor	Irvin Aerospace Inc.

Informational Websites

FEA Informationwebsites	www.feainformation.com
TopCrunch – Benchmarks	www.topcrunch.org
LS-DYNA Examples (more than 100 Examples)	www.dynaexamples.com
LS-DYNA Conference Site	www.ls-dynaconferences.com
LS-DYNA Publications to Download On Line	www.dynalook.com
LS-DYNA Publications	www.feapublications.com
LS-DYNA Forum	http://portal.ecadfem.com/Forum.1372.0.html
LS-DYNA CADFEM Portal	http://www.lsdyna-portal.com

Archived News Page

Feb. 07

- **Cray:** Cray X1 Supercomputer
- **MSC.Software** Gateway for LS-DYNA
- **FIGES** – Distributor, Turkey

Feb. 14

- **SGI**® Altix® 1350
- **The Japan Research Institute**, Limited is a "knowledge engineering" company
- **CADFEM GmbH** – Distributor, Germany

February 22

- **ETA:** The eta/VPG
- **Oasys**: Programs Environment
- **LEAP:** Distributor, Austrailia

February 28

- **AVI:** Added AVI #74 Casting
- **INTEL**: Technology and industry are poised for a broad transition to 64-bit computing.
- **HP**: HP's carrier-grade servers

WEBSITE REVIEW

Len Schwer, Ph.D.
6122 Aaron Ct.
Windsor CA 95492-8651
Voice: 707-837-0559
eFax: 928-833-1130
Home: 707-837-0958
Len@Schwer.net

SE&CS provides engineering services to Government and commercial clients. Services include the application and development of computational mechanics techniques with specializations in *nonlinear transient phenomena* and *constitutive modeling*.

Over 25 years of experience in the application, and development, of finite element analysis software. With a specialization in the application of the LSTC code LS-DYNA.

LS-DYNA EXPERIENCE AREAS Of Specialization

Geomaterials Modeling:

WWW.GEOMATERIALMODELING.COM

Rock, concrete, and soil are the three most common examples of geo-materials encountered in engineering applications. They are all characterized as 'frictional materials' in that their shear strength depends on the confinement of the material

Material Modeling

Material models, especially composite material modeling

Crashworthiness

Constructing and Evaluating Virtual Collisions of Vehicles

LSTC Short Course:
Modeling Geomaterials with LS-DYNA

Nov. 15-17

US$750 Early Registration
US$850 After Oct. 18
WWW.LSTC.COM -
TRAINING LINK

2004 - 8th LS-DYNA Conference Proceeding Publication

Preliminary Assessment of Non-Lagrangian Methods for Penetration Simulation

Computational Plasticity Part I: Basic Plasticity Theory

David J. Benson
Dept. of Mechanical and Aerospace Engineering
University of California, San Diego
dbenson@ucsd.edu

A material is said to have deformed plastically if it doesn't return to its original shape after the load is removed. The most common application for plasticity in finite element analysis is modeling the deformation of metals. While a great deal of research is available on the plasticity of metals at a very fundamental level, the majority of plasticity models are phenomenological and have no motivation beyond duplicating experimental data. The models discussed here are among the simpler plasticity models, and they are, indeed, completely phenomenological. While there are post hoc rationalizations of why these simple models perform as well as they do, they are still rationalizations.

1 The Tension Test

The most common mechanical test for characterizing metals is the tension test. A specimen is put in a machine which pulls it at a prescribed rate and simultaneously records the load on the specimen. The material is said to *yield* at the point where it stops behaving as an elastic material, and this point typically occurs at a small fraction of a percent of strain. After this point, if the load is removed, the specimen retains a permanent deformation called the *plastic deformation*. At some load the specimen breaks, and the test is over. Ductile metals *neck* at some point prior to failure. Until that point, the cross-sectional area of the specimen is uniform and very close to the original area before loading. The data are commonly plotted in two forms:

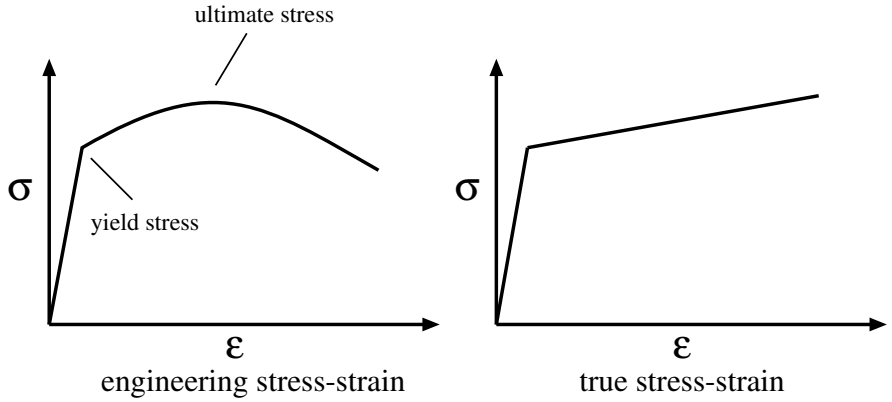

Figure 1: Engineering (left) and true (right) stress strain responses (not to scale).

1) engineering stress versus engineering strain, and 2) true stress versus true strain. Example plots, which aren't to scale, are shown in Figure 1.

The engineering stress, s, is the load, P, divided by the original cross-sectional area of the specimen, A_0, and the engineering strain, e, is the current length of the specimen, ℓ, divided by the original length, ℓ_0,

$$s = \frac{P}{A_0} \quad e = \frac{\ell}{\ell_0}. \tag{1}$$

In contrast, the true stress, σ, is the load divided by the current area, and the true strain, ϵ, is the log of the ratio of the original cross-sectional area to the current area at the neck,

$$\sigma = \frac{P}{A} \quad \epsilon = \log\left(\frac{A_0}{A}\right) \tag{2}$$

Once the specimen starts to neck, the strain is no longer uniform in the specimen. The true stress-true strain curve describes the response at the neck, where the stress is the highest. To calculate the true strain at the neck, an equivalent length ratio is calculated by assuming that the total volume of the specimen is constant during the test,

$$V = \ell_0 A_0 = \ell A \longrightarrow \frac{A_0}{A} = \frac{\ell}{\ell_0}. \tag{3}$$

Note that there is a peak in the engineering stress-strain plot, which is often referred to as the *ultimate strength* of the material. The true stress-strain plot, however, shows a steady increase in the stress after yielding to failure. A common approximation for the plastic portion of the true stress-strain curve is a straight line. In this simplified model, the *yield* or *flow* stress is a linear function of the plastic strain, $\bar{\epsilon}^p$,

$$\sigma_y = \sigma_y^0 + h\bar{\epsilon}^p. \tag{4}$$

The plastic hardening modulus, h, is typically orders of magnitude smaller than the elastic modulus, and if it is zero, the material is said to be *perfectly plastic*. An important restriction on the hardening modulus is that it must be greater than, or equal to, zero. If the hardening modulus is less than zero, then the material is softening and unstable. Real materials do exhibit softening, but an additional variable, the *damage* D, or temperature is necessary to model the softening effect correctly. Damage mechanics, which is an important area of continuum mechanics, is beyond the scope of this discussion.

The plastic strain is a *history* variable that evolves with the stress during the deformation of the material. An important distinction between the plastic strain and the material strain is that while a material may be stretched and compressed to produce both positive and negative material strains, the plastic strain is always greater than, or equal to, zero and never decreases, regardless of the deformation of the material.

2 The Equations for Isotropic von Mises Plasticity

The evolution of the stress is described by a system of differential equations,

$$\dot{\sigma}_{ij} = C_{ijkl}\dot{\epsilon}^e_{kl} \quad \dot{\boldsymbol{\sigma}} = \boldsymbol{C}\dot{\boldsymbol{\epsilon}}^e \tag{5}$$

where the superscript e stands for elastic. An additive decomposition of the strain rate into elastic and plastic parts (indicated by a superscript p) is assumed,

$$\dot{\boldsymbol{\epsilon}} = \dot{\boldsymbol{\epsilon}}^e + \dot{\boldsymbol{\epsilon}}^p \tag{6}$$

but it isn't unique; some formulations are based on a multiplicative decomposition of the deformation gradient into elastic and plastic parts. Using the

additive decomposition, and solving for the elastic strain rate, the stress rate is expressed as

$$\dot{\sigma}_{ij} = C_{ijkl}\left(\dot{\epsilon}_{kl} - \dot{\epsilon}^p_{kl}\right) \quad \dot{\boldsymbol{\sigma}} = \boldsymbol{C}\left(\dot{\boldsymbol{\epsilon}} - \dot{\boldsymbol{\epsilon}}^p\right) \tag{7}$$

This equation contains both the unknown stress rate and the unknown plastic strain rate. A model for the plastic strain rate is described later.

A basic goal of phenomenological plasticity models is to replicate the one-dimensional tension test. To achieve this, a scalar *equivalent stress*, $\bar{\sigma}$ is defined in terms of the stress tensor, an *equivalent plastic strain*, $\bar{\epsilon}^p$ is defined in terms of the plastic strain tensor, $\boldsymbol{\epsilon}^p$, and the equivalent stress is set equal to the yield stress,

$$\bar{\sigma}(\boldsymbol{\sigma}) = \sigma_y(\bar{\epsilon}^p). \tag{8}$$

Because a six-dimensional stress space is being collapsed into a single number, there are many stress states that will produce the same equivalent stress, and they collectively define a surface in stress space. The particular collection of stresses that satisfy Equation 8 define a *yield surface*, and the normal to the yield surface is defined as

$$\boldsymbol{n} = \frac{\partial\bar{\sigma}(\boldsymbol{\sigma})}{\partial\boldsymbol{\sigma}} \Big/ \left|\frac{\partial\bar{\sigma}(\boldsymbol{\sigma})}{\partial\boldsymbol{\sigma}}\right|. \tag{9}$$

Plastic flow occurs when the stress is on the yield surface and the stress rate points outside the yield surface,

$$\bar{\sigma}(\boldsymbol{\sigma}) = \sigma_y \quad \text{and} \quad \boldsymbol{n}^T\dot{\boldsymbol{\sigma}} > 0. \tag{10}$$

Inside the yield surface, $\bar{\sigma}(\boldsymbol{\sigma}) < \sigma_y$, the response is elastic regardless of the direction of the stress rate. When the response is elastic, the plastic strain rate is exactly zero, $\dot{\boldsymbol{\epsilon}}^p = 0$.

The choices for defining the equivalent stress and plastic strain aren't unique, but the choices made here are commonly used for modeling metals. The equivalent stress is the *von Mises* stress,

$$\bar{\sigma} = \sqrt{\frac{3}{2}\sigma'_{ij}\sigma'_{ij}} = \sqrt{\frac{3}{2}\boldsymbol{\sigma}' : \boldsymbol{\sigma}'}. \tag{11}$$

The superscript prime indicates the stress is the deviatoric stress, defined as

$$\sigma'_{ij} = \sigma_{ij} - \frac{\sigma_{kk}}{3}\delta_{ij} \quad \boldsymbol{\sigma}' = \boldsymbol{\sigma} - \frac{\mathrm{tr}(\boldsymbol{\sigma})}{3}\boldsymbol{I}. \tag{12}$$

For a one-dimensional uni-axial stress state ($\sigma_{11} = \sigma$ and all the other components are zero), the deviatoric stress is

$$\sigma'_{11} = (2/3)\sigma_{11}, \quad \sigma'_{22} = -(1/3)\sigma_{11}, \quad \sigma'_{33} = -(1/3)\sigma_{11} \tag{13}$$

with all the other stress components equal to zero. On substitution into Equation 11, the equivalent stress is

$$\bar{\sigma} = \sqrt{\frac{3}{2}\left\{\left(\frac{2}{3}\sigma_{11}\right)^2 + \left(-\frac{1}{3}\sigma_{11}\right)^2 + \left(-\frac{1}{3}\sigma_{11}\right)^2\right\}} = |\sigma_{11}|, \tag{14}$$

showing that the equivalent stress equals the magnitude of the uni-axial stress.

The equivalent plastic strain is the integral of the equivalent plastic strain rate,

$$\bar{\epsilon}^p = \int_0^t \dot{\bar{\epsilon}}^p \mathrm{d}t \tag{15}$$

and the equivalent plastic strain rate is defined in terms of the plastic strain rate,

$$\dot{\bar{\epsilon}}^p = \sqrt{\frac{2}{3}\dot{\epsilon}^p_{ij}\dot{\epsilon}^p_{ij}} = \sqrt{\frac{2}{3}\dot{\boldsymbol{\epsilon}}^p : \dot{\boldsymbol{\epsilon}}^p}. \tag{16}$$

Note that there is no prime on the plastic strain rate; the plastic strain rate tensor is deviatoric in this model by construction. Plastic flow in metals is *isochoric*, meaning that the volume of the material is unchanged by plastic flow, which corresponds to a Poisson's ratio of 0.5. For uni-axial stress, the plastic strain rate has the form

$$\dot{\epsilon}^p_{11} = \dot{\epsilon}, \quad \dot{\epsilon}^p_{22} = -\frac{1}{2}\dot{\epsilon}, \quad \dot{\epsilon}^p_{33} = -\frac{1}{2}\dot{\epsilon} \quad \text{therefore} \quad \sum_{i=1}^{3} \dot{\epsilon}^p_{ii} = 0 \tag{17}$$

and all the shear strain rates are zero. The terms sum to zero, demonstrating that the plastic strain rate is deviatoric. Substituting in this plastic strain rate into Equation 16,

$$\dot{\bar{\epsilon}}^p = \sqrt{\frac{2}{3}\left\{(\dot{\epsilon}^p)^2 + \left(-\frac{1}{2}\dot{\epsilon}^p\right)^2 + \left(-\frac{1}{2}\dot{\epsilon}^p\right)^2\right\}} = |\dot{\epsilon}^p|, \tag{18}$$

demonstrating that the multi-dimensional strain rate reduces to the one-dimensional plastic strain rate.

Drucker postulated *associated flow*, which says that the plastic strain rate is parallel to the normal to the yield surface,

$$\dot{\boldsymbol{\epsilon}}^p = \Lambda \boldsymbol{n} \tag{19}$$

where Λ is a proportionality constant that must be determined to complete the plasticity model. The proportionality constant Λ is always greater than, or equal to zero, because a negative value implies that the response is elastic. The relation between $\dot{\bar{\epsilon}}^p$ and Λ is obtained by substituting in the definition of the plastic strain rate into the definition of the equivalent plastic strain rate,

$$\dot{\bar{\epsilon}}^p = \sqrt{\frac{2}{3}}\Lambda. \tag{20}$$

For the von Mises equivalent stress, the normal is

$$n_{ij} = \frac{\sqrt{3/2}}{\bar{\sigma}}\sigma'_{ij} \quad \boldsymbol{n} = \frac{\sqrt{3/2}}{\bar{\sigma}}\boldsymbol{\sigma}'. \tag{21}$$

For linear, isotropic elasticity, expressed in terms of the Lame constants μ and λ, the stress rate equation becomes

$$\begin{aligned} \dot{\sigma}_{ij} &= 2\mu\left(\dot{\epsilon}'_{ij} - \Lambda \boldsymbol{n}_{ij}\right) + (\lambda + \frac{2}{3}\mu)\dot{\boldsymbol{\epsilon}}_{kk}\delta_{ij} \\ \dot{\boldsymbol{\sigma}} &= 2\mu\left(\dot{\boldsymbol{\epsilon}}' - \Lambda \boldsymbol{n}\right) + (\lambda + \frac{2}{3}\mu)\mathrm{tr}(\dot{\boldsymbol{\epsilon}})\boldsymbol{I} \end{aligned} \tag{22}$$

Substituting in the results of Equation 20 gives

$$\begin{aligned} \dot{\sigma}_{ij} &= 2\mu\left(\dot{\epsilon}'_{ij} - \sqrt{\frac{3}{2}}\dot{\bar{\epsilon}}^p \boldsymbol{n}_{ij}\right) + (\lambda + \frac{2}{3}\mu)\dot{\boldsymbol{\epsilon}}_{kk}\delta_{ij} \\ \dot{\boldsymbol{\sigma}} &= 2\mu\left(\dot{\boldsymbol{\epsilon}}' - \sqrt{\frac{3}{2}}\dot{\bar{\epsilon}}^p \boldsymbol{n}\right) + (\lambda + \frac{2}{3}\mu)\mathrm{tr}(\dot{\boldsymbol{\epsilon}})\boldsymbol{I} \end{aligned} \tag{23}$$

The first term to the right of the equals sign defines the evolution of the deviatoric stress, while the second term governs the mean stress, which is the negative of the pressure, P. Note that the mean stress doesn't appear in the definition of the equivalent stress and its evolution isn't a function

of the plastic strain rate. This allows the evolution of the deviatoric and mean stresses to be considered independently. A different definition of the equivalent stress (or equivalently, the yield surface) can lead to coupling between all the terms.

To summarize the plasticity model, if the response is elastic, then

$$\dot{\boldsymbol{\sigma}}' = 2\mu\dot{\boldsymbol{\epsilon}}' \tag{24}$$

$$\dot{P} = -(\lambda + \frac{2}{3}\mu)\mathrm{tr}(\dot{\boldsymbol{\epsilon}}) \tag{25}$$

$$\dot{\bar{\epsilon}}^p = 0. \tag{26}$$

and if it is plastic, then

$$\dot{\boldsymbol{\sigma}}' = 2\mu\left(\dot{\boldsymbol{\epsilon}}' - \sqrt{\frac{3}{2}}\dot{\bar{\epsilon}}^p\boldsymbol{n}\right) \tag{27}$$

$$\dot{P} = -(\lambda + \frac{2}{3}\mu)\mathrm{tr}(\dot{\boldsymbol{\epsilon}}) \tag{28}$$

$$\dot{\sigma}_y = h\dot{\bar{\epsilon}}^p \tag{29}$$

$$\dot{\bar{\epsilon}}^p = \sqrt{\frac{3}{2}}\Lambda. \tag{30}$$

3 The Consistency Condition

An expression for Λ in terms of the stress and strain rate is required in Equation 30 to complete the plasticity model.

Differentiating Equation 8 with time gives the *consistency condition*, which defines Λ.

$$\dot{\bar{\sigma}} = \left(\frac{\partial\bar{\sigma}}{\partial\boldsymbol{\sigma}}\right)^T \boldsymbol{C}\left(\dot{\boldsymbol{\epsilon}} - \Lambda\boldsymbol{n}\right) = \dot{\sigma}_y \tag{31}$$

For linear hardening,

$$\dot{\sigma}_y = h\dot{\bar{\epsilon}}^p = \sqrt{\frac{2}{3}}h\Lambda. \tag{32}$$

Noting that $\partial\bar{\sigma}/\partial\boldsymbol{\sigma} = \sqrt{3/2}\boldsymbol{n}$ for the von Mises equivalent stress, the expression for Λ simplifies to

$$\Lambda = \frac{\boldsymbol{n}^T\boldsymbol{C}\dot{\boldsymbol{\epsilon}}}{\boldsymbol{n}^T\boldsymbol{C}\boldsymbol{n} + \frac{2}{3}h}. \tag{33}$$

4 The Continuum Tangent Matrix for Plastic Flow

Substituting Equations 33 and 20 into Equation 7 gives the continuum tangent matrix,

$$\frac{\partial \dot{\sigma}_{ij}}{\partial \dot{\epsilon}_{kl}} = C_{ijkl} - \frac{(C_{ijmn} n_{mn})(n_{ab} C_{abkl})}{n_{qr} C_{qrst} n_{st} + \frac{2}{3} h} \tag{34}$$

$$\frac{\partial \dot{\boldsymbol{\sigma}}}{\partial \dot{\boldsymbol{\epsilon}}} = \boldsymbol{C} - \frac{(\boldsymbol{C}\boldsymbol{n}) \otimes (\boldsymbol{n}^T \boldsymbol{C})}{\boldsymbol{n}^T \boldsymbol{C} \boldsymbol{n} + \frac{2}{3} h} \tag{35}$$

For isotropic elasticity,

$$\boldsymbol{C}\boldsymbol{n} = 2\mu \boldsymbol{n} \tag{36}$$

which allows the elasto-plastic tangent matrix to be simplified to

$$\frac{\partial \dot{\sigma}_{ij}}{\partial \dot{\epsilon}_{kl}} = C_{ijkl} - \frac{6\mu^2}{3\mu + h} n_{ij} n_{kl} \tag{37}$$

$$\frac{\partial \dot{\boldsymbol{\sigma}}}{\partial \dot{\boldsymbol{\epsilon}}} = \boldsymbol{C} - \frac{6\mu^2}{3\mu + h} \boldsymbol{n} \otimes \boldsymbol{n} \tag{38}$$

where $\boldsymbol{C}$ is the standard linear isotropic elasticity matrix. This tangent is only used when there is plastic flow, and the elastic tangent is used otherwise.